Synthesis and characterization of Ag-ion-exchanged zeolite/TiO2 nanocomposites for antibacterial applications and photocatalytic degradation of antibiotics

Torkian, Niloufar ; Bahrami, Abbas; Hosseini-Abari, Afrouzossadat; Momeni, Mohammad Mohsen ; Abdolkarimi-Mahabadi, Meisam ; Bayat, Ahmad ; Hajipour, Pejman ; Rourani, Hamed Amini; Yazdan Mehr, Maryam; More Authors

DOI
10.1016/j.envres.2021.112157

Publication date
2022

Document Version
Final published version

Published in
Environmental Research

Citation (APA)
Torkian, N., Bahrami, A., Hosseini-Abari, A., Momeni, M. M., Abdolkarimi-Mahabadi, M., Bayat, A., Hajipour, P., Rourani, H. A., Yazdan Mehr, M., & More Authors (2022). Synthesis and characterization of Ag-ion-exchanged zeolite/TiO2 nanocomposites for antibacterial applications and photocatalytic degradation of antibiotics. *Environmental Research*, *207*, Article 112157. https://doi.org/10.1016/j.envres.2021.112157

Environmental Research 207 (2022) 112157

Contents lists available at ScienceDirect

Environmental Research

journal homepage: www.elsevier.com/locate/envres

Synthesis and characterization of Ag-ion-exchanged zeolite/TiO_2 nanocomposites for antibacterial applications and photocatalytic degradation of antibiotics

Niloufar Torkian [a], Abbas Bahrami [b,**], Afrouzossadat Hosseini-Abari [c], Mohammad Mohsen Momeni [d], Meisam Abdolkarimi-Mahabadi [a], Ahmad Bayat [a], Pejman Hajipour [b], Hamed Amini Rourani [c], Mohammad Saeid Abbasi [b], Sima Torkian [b], Yangping Wen [e], Maryam Yazdan Mehr [f], Akbar Hojjati-Najafabadi [g,h,*]

[a] Department of Chemical Engineering, Tafresh University, Tafresh 79611-39518, Iran
[b] Department of Materials Engineering, Isfahan University of Technology, Isfahan 84156-83111, Iran
[c] Department of Cell and Molecular Biology and Microbiology, Faculty of Biological Science and Technology, University of Isfahan 817463441, Iran
[d] Department of Chemistry, Isfahan University of Technology, Isfahan 84156-83111, Iran
[e] Institute of Functional Materials and Agricultural Applied Chemistry, Jiangxi Agricultural University, Nanchang, 330045, China
[f] Faculty EEMCS, Delft University of Technology, Mekelweg 4, 2628 CD Delft, the Netherlands
[g] College of Rare Earths, Jiangxi University of Science and Technology, No.86, Hongqi Ave., Ganzhou, Jiangxi, 341000, PR China
[h] Faculty of Materials, Metallurgy and Chemistry, School of Materials Science and Engineering, Jiangxi University of Science and Technology, Ganzhou, 341000, PR China

ARTICLE INFO

Keywords:
Catalyst
Natural zeolite
Antibacterial
TiO_2
Antibiotic
Amoxicillin

ABSTRACT

This paper investigates the synthesis, antibacterial, and photocatalytic properties of silver ion-exchanged natural zeolite/TiO_2 photocatalyst nanocomposite. Zeolite is known to have a porous surface structure, making it an ideal substrate and framework in different nanocomposites. Moreover, natural zeolite has a superior thermal and chemical stability, with hardly any reactivity with chemicals. Finding an effective and low-cost method to remove both antibiotics and bacteria from water resources has become a vital global issue due to the worldwide excessive use of chemicals and antibiotics. This research aims to propose a facile method to synthesize Ag-ion-exchanged zeolite/TiO_2 catalyst for anti-bacterial purposes and photocatalytic removal of atibiotics from wastewaters. TiO_2 particles were deposited on the surface of natural zeolite. Ag ion exchanging was performed via a liquid ion-exchange method using 0.1 M $AgNO_3$ solution. X-ray diffractometry (XRD), scanning electron microscopy (SEM), energy-dispersive X-ray spectroscopy (EDS), and Fourier-transform infrared spectroscopy (FTIR) were used to evaluate the structure of synthesized powders. Antibacterial activities of samples were assessed, using *Staphylococcus aureus* ATCC 25923 and *Escherichia coli* ATCC 25922 by disc diffusion method. It was shown that Ag-containing nanocomposite samples have an improved antibacterial performance in both cases. Results showed that the synthesized catalyst has promising potentials in wastewater treatment.

1. Introduction

Recently, hospital wastewater treatment has become a critical issue due to its harmful and devastating effects on the ecosystem and the environment. Presence of different bacteria and the emergence and excessive use of a variety of antibiotics such as penicillin, diphenhydramine and amoxicillin in hospitals have made hospital wastewater a very complicated and dangerous disposal. Antibiotics produce toxicity and resistant against bacteria in natural waters (Li et al., 2019; Karimi-Maleh et al., 2021a, 2021b; Bergamonti et al., 2019; Doan et al., 2021). Therefore, it is important to employ highly efficient, low-cost, and multi-functional strategies to eliminate biological and medical pollutants from the wastewater (Wen et al., 2004; Jalbani et al., 2021; Beier et al., 2011; Hajipour et al., 2021; Verlicchi et al., 2010;

* Corresponding author. College of Rare Earths, Jiangxi University of Science and Technology, No.86, Hongqi Ave., Ganzhou, Jiangxi, 341000, PR China.
** Corresponding author.
E-mail addresses: a.n.bahrami@iut.ac.ir (A. Bahrami), a_hojjati@jxust.edu.cn, a_hojjati@yahoo.com (A. Hojjati-Najafabadi).

https://doi.org/10.1016/j.envres.2021.112157
Received 24 July 2021; Received in revised form 16 September 2021; Accepted 26 September 2021
Available online 4 October 2021

Karimi-Maleh et al., 2020a). Zeolite, a hydrated aluminosilicates mineral of alkali/alkaline-earth metals, has recently gained lots of attention as a cheap and widely available natural mineral (Alswat et al., 2017). The crystal structure of zeolite consists of interconnected $[A1O_4]^{5-}$ and $[SiO_4]^{4-}$ units, which are linked via sharing an oxygen atom. Zeolite also normally contains Ca^{2+}, K^{+}, and Na^{+} cations, which are placed inside cavities in the crystal structure. An important upside with zeolite is the uniform existence of channels and pores in this mineral. That is why zeolite is known to have an excellent absorption ability, clearly due to its high surface-to-volume ratio. This not only significantly enhances the surface absorption of zeolite, but also improves the bonding/anchoring of nano-sized particles over its surface. Moreover, this mineral has a superior thermal and chemical stability, with hardly any reactivity with chemicals, making it an ideal option for a support framework in anti-bacterial nanocomposites (Zhang et al., 2018). It is reported that TiO_2 nanoparticles, grown on zeolite, show an enhanced photocatalytic activity and higher stability, which has to do with the formation of Ti–O–Al and Ti–O–Si bonds over the surface (Ren et al., 2010; Mansoorianfar et al., 2021). Further improvement in this direction is using a treated zeolite with extra functionality in addition to its role as the holding support for nanoparticles. That gives an extra added-value to zeolite. The addition of nanoparticles, like copper, gold, and silver to zeolite crystal structure can give anti-bacterial properties to zeolite. The latter element is long known as an element with perfect anti-bacterial characteristics (Ren et al., 2010; Hajipour et al., 2012; Wu and Tseng, 2006; Bai et al., 2011; Orooji et al., 2021).

Amoxicillin (*AMX*), one of the most common β-lactam antibiotics, is known to have chemical stability, low rate of degradation and high level of toxicity. Concerns have raised in last few years on the grounds that *AMX* has been traced back in environmental samples and detected in rivers and surface waters. That and the fact that *AMX* is one of the most widely used antibiotics have put a lot of pressure on hospitals to remove it from their wastewaters (Bergamonti et al., 2019; Verlicchi et al., 2010; Dimitrakopoulou et al., 2012; Sadrnia et al., 2021). Owing to the mentioned emerging demand, *AMX* was chosen as a model drug contaminant.

This research aims to synthesize an Ag-ion-exchanged zeolite/TiO_2 catalyst for anti-bacterial and photocatalytic purposes. The idea is to propose a method to fix nano-sized TiO_2 particles on a zeolite framework, which is also activated by entering Ag ions into its structure. So, this is more a hybrid system, in which each component has anti-bacterial and photocatalytic characteristic. The environmental contaminants, industrial wastes, hospital wastewater and organic pollutants are getting increasingly complicated. This necessitates using highly functional hybrid disinfection methods, based on nanocomposite materials. The novelty of this research is the modification of natural zeolite using Ag-ion-exchange, and TiO_2 deposition for the development of a low-cost catalyst powder for simultaneous degradation of antibiotics and bacteria in a simulated hospital wastewater.

2. Materials and methods

2.1. Synthesis of Ag-ion-exchanged zeolite/TiO_2 catalyst

To deposit nano-sized TiO_2 particles on natural zeolite powders (Natural zeolite, Semnan Zeolite Mine, 1–20 μm), hydrolysis of Titanium (IV) isopropoxide (TTIP, 97%, Sigma-Aldrich) was used. First, zeolite particles were sonicated in an ultrasonic bath in ethanol for 15 min to eliminate surface impurities and contaminants. Then, 3 g of rinsed/dried natural zeolite was added to 200 ml aqua solution of ethanol 50% (V/V). Four different amounts (0.1, 0.3, 0.5, and 1 ml) of Titanium (IV) isopropoxide were added to the prepared solution. Table 1 shows the coding used for these samples. Colloidal solutions were then stirred at room temperature for 24 h. A magnetic stirrer with 400 rpm was used for this purpose. The stirring was carried out to make sure that a complete hydrolysis/condensation of TTIP was attained. Powdered samples were dried in an oven at 75 °C for 3 h, followed by calcination at 500 °C for 3 h. Silver-ion-exchanging was performed via a liquid ion-exchange method. In this method, the prepared zeolite-TiO_2 composite powders were added to 100 ml solutions of 0.1 M silver nitrate ($AgNO_3$, ≥99.0%, Sigma Aldrich), dissolved in deionized water with a 1:20 wt ratio. The obtained solution was then stirred at room temperature for 48 h. Ion-exchanged powders were then dried at 75 °C for 3 h.

Table 1
Sample coding in this study.

Code	TTIP amount (ml)	Solution amount (ml)
ZT1	0.1	200
ZT2	0.3	200
ZT3	0.5	200
ZT4	1	200

2.2. Characterization

X-ray diffractometry (XRD) (Philips diffractometer, 40 kV, Cu(Kα) = 0.15406 nm, step size: 0.05°/1 s, Eindhoven, the Netherland) was used to evaluate the phase composition of synthesized samples. XRD patterns were assessed and interpreted by PANalytical X'Pert High Score software. Scanning electron microscope (SEM, Philips XI30, Eindhoven, The Netherlands), energy-dispersive X-ray spectroscopy (EDS, Seron AIS 2300, Seoul, South Korea), and Fourier-transform infrared spectroscopy (FTIR, Bruker Tensor 27) were utilized to characterize the synthesized catalyst samples. The specific surface area and pore size distribution of bare zeolite and the synthesized catalyst samples were evaluated by N_2 adsorption-desorption isotherms (Beishide 3H–2000PS2, Beijing, China).

2.3. Antibacterial activity

Antibacterial activities of prepared samples were assessed using *Staphylococcus aureus* ATCC 25923 and *Escherichia coli* ATCC 25922 by disc diffusion method. For the growth inhibition measurements, 100 μL of a fresh culture was spread on nutrient agar plates. The saturated paper disks, containing 10 mg/ml natural zeolite-TiO_2 and silver ion-exchanged natural zeolite-TiO_2 catalysts, were irradiated for 30 min using a UV chamber, then placed in the medium. The UV irradiation of samples would activate the antibacterial mechanisms of TiO_2 structures and also eliminates the risk of bacterial contamination of the disc diffusion test. A blank disk was used as a reference sample. The inhibition zone was measured after 24 h of incubation at 37 °C. Each reported inhibition zone, corresponding to each catalyst sample, was the result of three measurements.

2.4. Photocatalytic degradation experiments

One g/L Amoxicillin (*AMX*)/de-ionized water solution was used to assess the photocatalytic behavior of natural Zeolite, ZT1, and ZT3 samples. For this aim, 0.01 g of powder was added to 15 ml of *AMX* solution (pH = 6.7 at room temperature). Solutions were then slowly stirred for 30 min in a dark chamber to ensure that photocatalysts powders and *AMX* were very well mixed and in equilibrium. After that, solutions were exposed to light under UV light located 20 cm above the stirring solutions (400 W high-pressure Hg lamp with an intensity of 120 mW cm^2). While exposed to light, samples were constantly stirred.

3. Results and discussion

3.1. SEM/EDS analyses of synthesized zeolite/TiO_2 samples

Fig. 1 depicts SEM micrographs of ZT1 and ZT4 samples. Natural zeolite particles have irregular morphologies with a relatively wide size

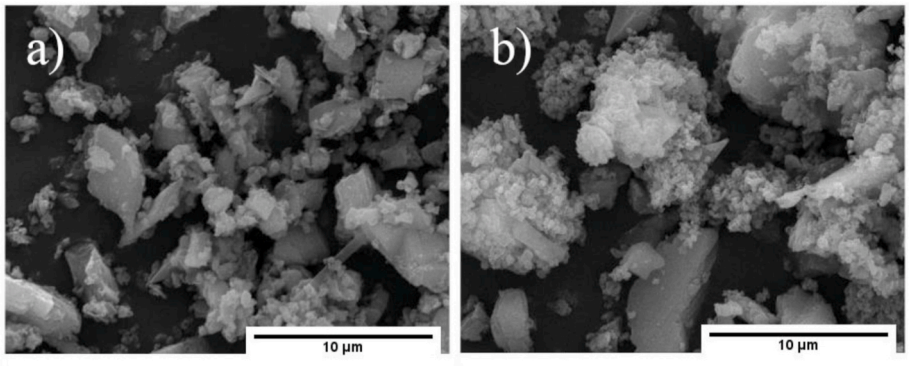

Fig. 1. SEM micrographs of a) ZT1 and b) ZT4 samples.

distribution. The plate-like morphology is indeed very useful, as it provides rather large nucleation sites for the precipitation of TiO_2 particles. The major difference between ZT1 and ZT4 samples is the amount of TTIP, used in the synthesis. The latter sample is synthesized with a higher content of TTIP, resulting in a higher content of TiO_2 in the final composite mixture. As it can be seen in Fig. 1, TiO_2 particles have nucleated on zeolite platelets. In some areas, large clusters of TiO_2 particles, with their size being a few micrometers, are noticeable. It appears that TiO_2 particles have a rather narrow size distribution. EDS analyses were performed on three different areas: i) platelets of natural zeolite, ii) isolated particles on zeolite platelets, and iii) particle clusters, as shown in Fig. 2. According to EDS analyses, the main structural elements of natural zeolite are oxygen and calcium, as expected. EDS analyses of isolated and clustered particles on zeolite platelets confirm that particles in both cases are TiO_2. The EDS elemental mapping available elements in the ZT4 synthesized sample is shown in Fig. 3, showing that elements are homogeneously distributed.

3.2. XRD analyses of synthesized samples

Fig. 4 depicts XRD patterns for synthesized samples. Peaks at 2θ: 23.3, 30, and 32° indicate that samples were mainly clinoptilolite with monoclinic crystallographic structure (Zhang et al., 2018; Treacy and Higgins, 2007; Gawande et al., 2012). As is the case for most natural zeolites, some percentages of calcium carbonate are also present in the samples. Peaks indicating the trigonal structure of $CaCO_3$ are shown in Fig. 4. The average crystallite size, calculated using Scherer formula (Patterson, 1939; HojjatiNajafabadi et al., 2016a), was 42 nm for clinoptilolite natural zeolite samples and 55 nm for the deposited TiO_2. Increasing the amount of TiO_2 on the natural zeolite surface does not affect peak positions in the XRD pattern. This result is in good agreement with previous research (Liu et al., 2014). Indexed peaks referring to $CaCO_3$ coincide with the standard *JCPDS* (card no: 96-450-2444), indicating the existence of $CaCO_3$ with hexagonal crystallographic structure as impurities in the natural zeolite samples. Enlarged graphs of XRD patterns depict the characteristic peak at 2θ: 25.3° in all samples, which correspond to the (1 0 1) plane in anatase TiO_2, indicating that TiO_2 has been deposited on the natural zeolite samples. Peaks ascribed to TiO_2, are in good agreement with the standard *JCPDS* (card no: 96-101-0943), which indicates the formation of anatase TiO_2 with a tetragonal crystallographic structure.

3.3. FTIR analyses of synthesized samples

Fig. 5 depicts the FTIR spectra for natural clinoptilolite zeolite and the ZT3 sample. The absorption band at 875 cm^{-1} corresponds to Ti═O stretching vibrations. The increase in the peak intensity in TiO_2-containing sample again approves that TiO_2 structure was successfully incorporated into the zeolite. It is also indicated that Ti species are

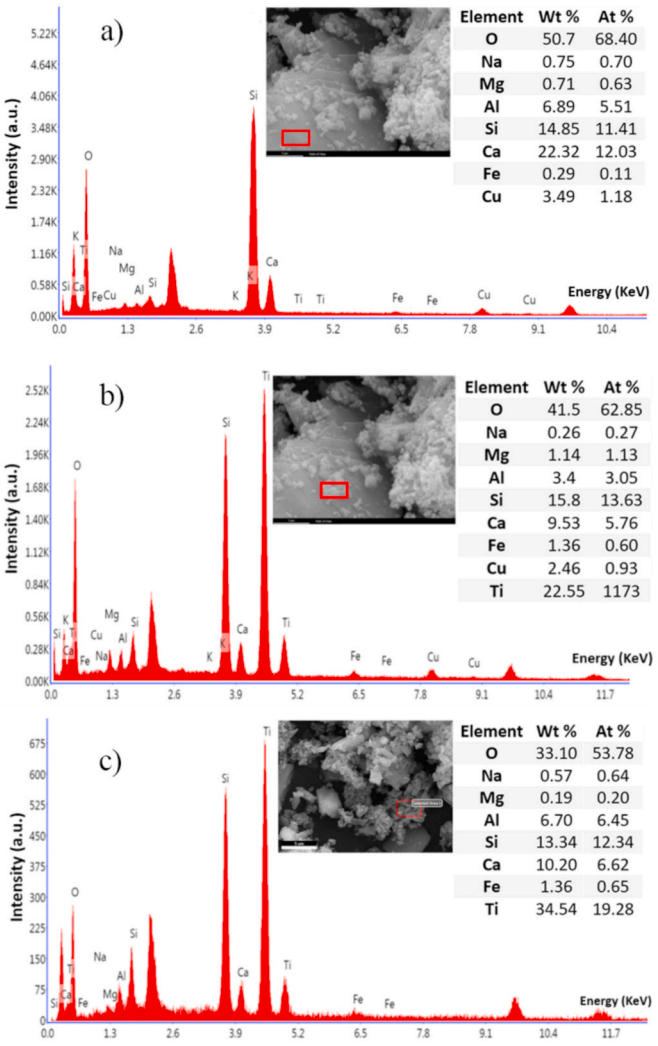

Fig. 2. EDS analyses of a) natural zeolite, b) isolated particles, and c) colonies of particles.

directly attached to Si framework due to the slight variation of the Ti–O–Ti (Ti–O–Si and/or Ti–O–Al) tensile vibrations from the framework (1013 cm^{-1} to 1036 cm^{-1}). As a result of the pores in the zeolite structure, the amount of TiO_2 on the zeolite increased. Also, the change in the spectrum shape in the range of 600–790 cm^{-1} shows that TiO_2 interacts with the pore network of zeolite (Song et al., 2017; Rahman et al., 2018). Hardly any significant change was observed in the range

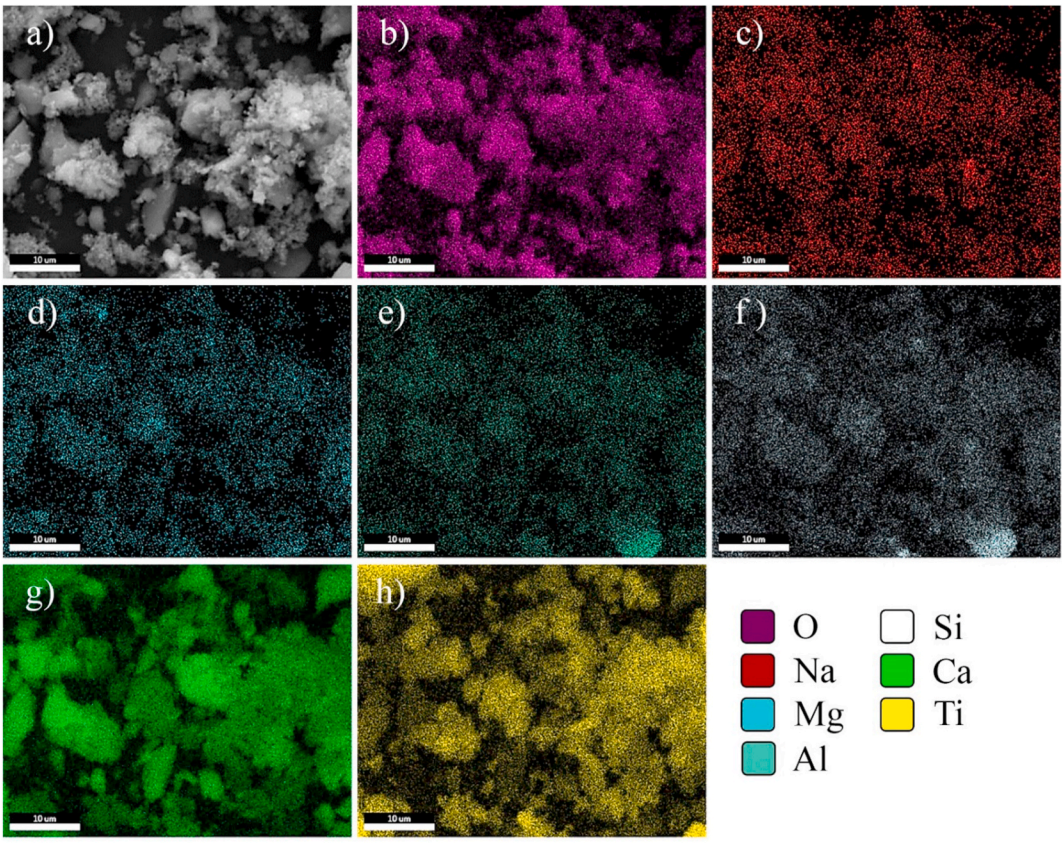

Fig. 3. a) SEM micrograph and elemental mapping of *ZT4* sample, showing the distribution of b) O, c) Na, d) Mg, e) Al, f) Si, g) Ca, and h) Ti elements.

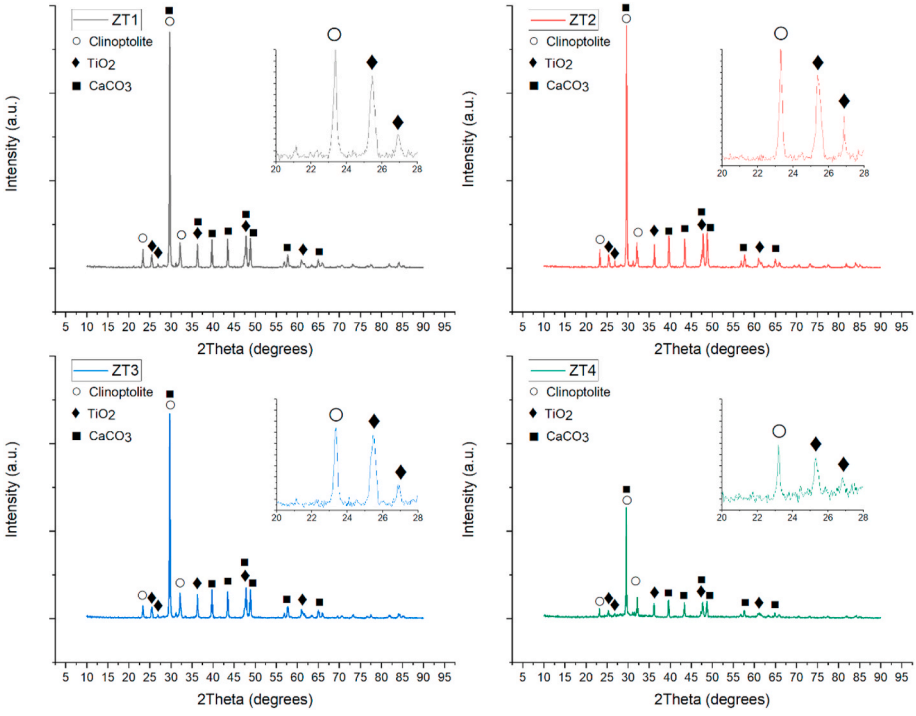

Fig. 4. XRD patterns of zeolite-TiO_2 synthesized by hydrolysis of TTIP.

between 2800 and 3500 cm^{-1}, which is mainly attributed to the H_2O and CO_2 molecules adsorbed on the zeolite surface. In addition, the peaks at 1443 cm^{1} and 2515 cm^{-1} are attributed to the existence of antisymmetric stretching bonds of $CaCO_3$ (HojjatiNajafabadi et al., 2016b; Huang et al., 2020; Lavat and Grasselli, 2015; Cheraghi et al., 2021; Brundha et al., 2017). Furthermore, the widespread peaks

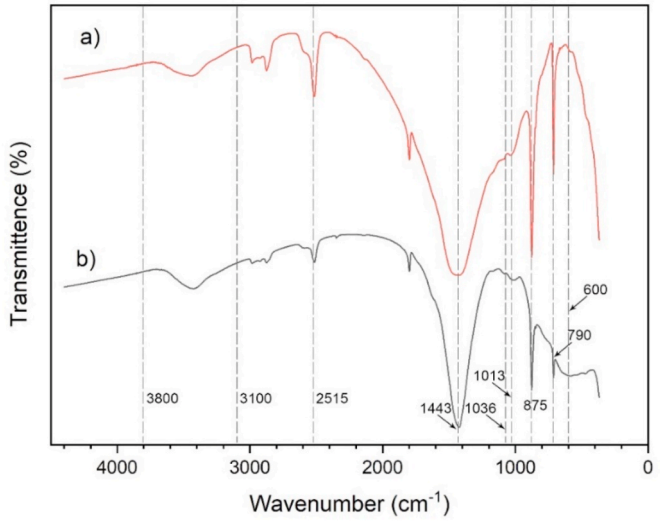

Fig. 5. FTIR analysis for a) natural zeolite b) zeolite-TiO_2 (ZT3) composite synthesized by hydrolysis of TTIP.

between 3100 and 3800 cm^{-1} are related to O–H tensile vibration, which can be ascribed to a small amount of H_2O (Hajipour et al., 2020; Najafabadi et al., 2013; Mahmoodi et al., 2020).

3.4. SEM/EDS analyses of Ag-ion-exchanged zeolite/TiO_2 samples

Figs. 6 and 7 depict Ag-ion-exchanged zeolite/TiO_2 catalyst. White phases, distributed within zeolite particles, are rich in silver, as shown in Fig. 6. It appears that silver particles are perfectly homogeneously distributed within zeolite particles. Moreover, Ag-containing particles have a rather narrow size distribution. As seen in Fig. 7b, Ag ions are also well dispersed inside the zeolite structure, indicating that a perfect Ag ion replacement has been achieved.

3.5. BET surface area analyses

The nitrogen adsorption-desorption isotherms of natural zeolite and silver ion-exchanged natural zeolite/TiO_2 catalysts are depicted in Fig. 8. According to BDDT (Brunauer, Deming, Deming, and Teller), the isotherms are typical type IV irotherms (Sing, 1985). A hysteresis loop (type H3) can be seen in all samples, indicating that structures are mesoporous (Liao et al., 2018). As shown in Fig. 8, the isotherms of the natural zeolite were different from those of TiO_2 containing samples, meaning that after TiO_2 was deposited on the surface of the natural zeolite, it changes the specific surface area. As presented in Table 2, the results showed that the TiO_2 formation on the surface of natural zeolite samples resulted in the reduction of BET specific surface area and total

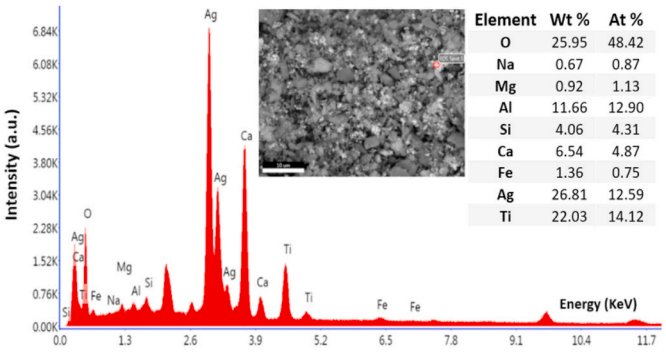

Element	Wt %	At %
O	25.95	48.42
Na	0.67	0.87
Mg	0.92	1.13
Al	11.66	12.90
Si	4.06	4.31
Ca	6.54	4.87
Fe	1.36	0.75
Ag	26.81	12.59
Ti	22.03	14.12

Fig. 6. EDS analysis of Ag-ion-exchanged zeolite-TiO_2 catalyst.

pore volume, contrasted to that of the bare natural zeolite (Foura et al., 2017). The pore volume and average pore size of zeolite samples showed a slight reduction due to the TiO_2 loading process. This confirmed that TiO_2 particles were immobilized on the surface of the zeolite resulting in a partial blockage of surface pores of bare natural zeolite samples.

3.6. Anti-bacterial characteristics of synthesized specimens

The obtained results for the anti-bacterial activity of silver ion-exchanged natural zeolite/TiO_2 catalysts are depicted in Fig. 9. The diameter of the zone of inhibition indicates the sensitivity of the bacteria against tested samples. According to the disc diffusion test results, shown in Fig. 9, all samples have antibacterial behavior against gram-positive *Staphylococcus aureus* and gram-negative *Escherichia coli*. This is due to the combined photocatalytic antibacterial properties of synthesized anatase TiO_2, which has been regarded as an antimicrobial material, and silver ions placed in the natural zeolite. Anti-bacterial properties of TiO_2 nanostructures as photocatalytic nanomaterials have widely been studied and reported (Kim et al., 2013; Bai et al., 2013; Pelaez et al., 2012; Yue et al., 2014) under visible and UV light irradiation, TiO_2 nanoparticles are known to result in the formation of Reactive Oxygen Species (ROS) which are reactive species with strong positive redox potential, and free radicals on the membrane surface or in the intracellular cytoplasm of the bacteria, resulting in the disruption of the membrane protein activity, which in turn leads to the demise of the microorganism (Kim et al., 2013; Nadtochenko et al., 2005). Reactions resulting in the formation of ROS in TiO_2 nanoparticles are given as follows:

$$TiO_2 + h\nu \rightarrow h^+_{VB} + e^-_{CB} \quad (1)$$

$$e^-_{CB} + O_2 \rightarrow O^{\bullet}{}_2^- \quad (2)$$

$$O^{\bullet}{}_2^- + H^+ \rightarrow HOO^{\bullet} \quad (3)$$

$$O_2^{\bullet -} + e^-_{CB} + 2H^+ \rightarrow H_2O_2 \quad (4)$$

$$HO_2^{\bullet} + 2\,e^-_{CB} + H^+ \rightarrow OH^{\bullet} + OH^- \quad (5)$$

The bactericidal effects of Ag nanoparticles and Ag ions have also been widely studied (Ghasemi et al., 2018; Karimi-Maleh et al., 2021c; Hosseini-Abari et al., 2014; Hojjati-najafabadi et al., 2021; Karimi-Maleh et al., 2020b). Previous studies showed that Ag ions have high bactericidal effects on pathogenic bacteria such as *E.coli, Klebsielapneumoniae*, *Pseudomonas aeruginosa*, *Streptococcus mutans*, *Streptococcus sobrinus,* and *S. aureus* (Hosseini-Abari et al., 2014; Morones et al., 2005; Shahin and Bouzari, 2018). The antibacterial mechanism of silver in bacteria varies with changes in physiology or chemical composition of the membrane and intercellular components. In *E.coli*, Ag ions reportedly disturb the permeability of the cell wall, respiration, and cell division. Silver ions also interact with the cell membrane and phosphorus- and sulfur-containing compounds resulting in disruption of cell activity and eventually its death (Morones et al., 2005). And, in *S. aureus*, ROS generation together with electrostatic interactions and physical damage of bacteria have been reported as major antibacterial mechanisms of silver ions (Hajipour et al., 2012). As clearly seen in Fig. 9, the increase in the TiO_2 content of catalyst samples is associated with an increased antibacterial performance of catalysts in both gram-positive *Staphylococcus aureus* ATCC 25923 and gram-negative *Escherichia coli* ATCC 25922. This infers a synergic effect between photocatalytic antibacterial behavior of deposited TiO_2 and silver ions in the natural zeolite. In the modified silver ion-exchanged natural zeolite/TiO_2 catalysts, zeolite has a high adsorption ability owing to its large surface area (as already seen in the BET analysis results in Table 2). Due to this high adsorption ability of zeolite, free radicals, and the produced ROS on the surface of TiO_2 nanostructures can easily transfer onto the surface of the natural zeolite. This infers that the surface of zeolite-based catalyst structure in this case has become highly antibacterial against different pathogens. It can also

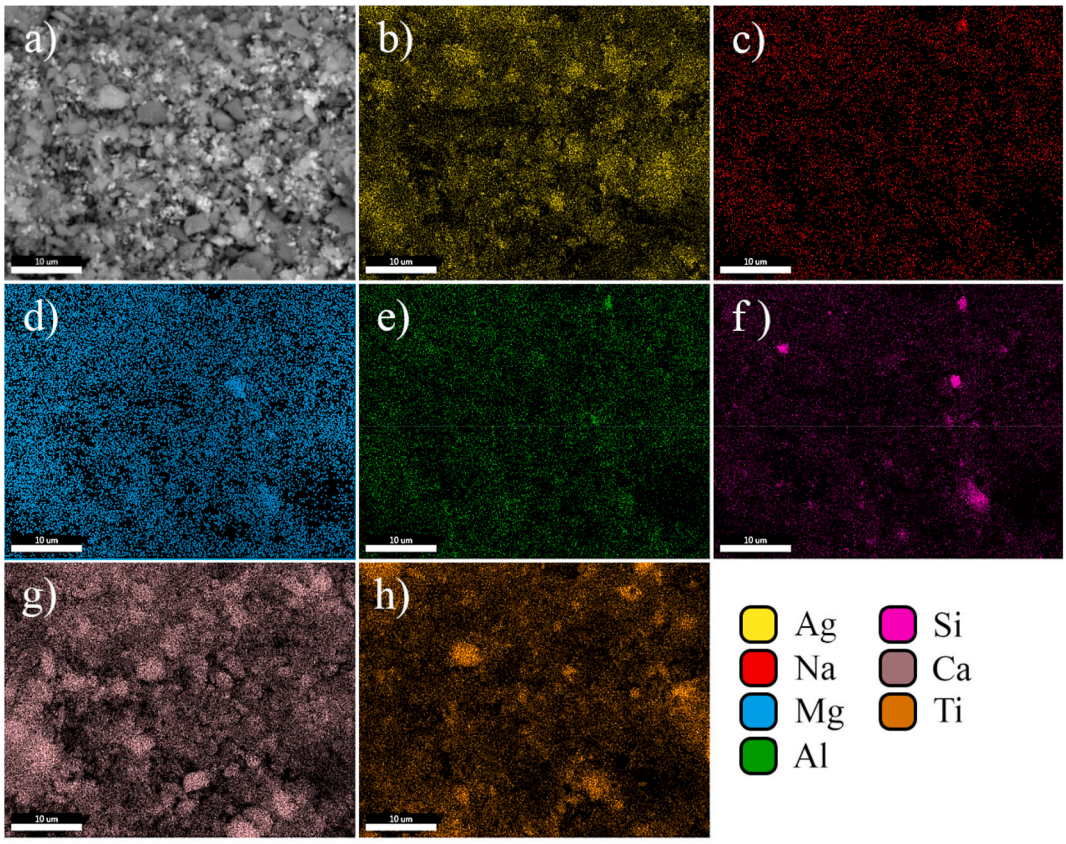

Fig. 7. a) SEM micrograph and elemental mapping of ZT4 ion-exchanged sample, showing the distribution of b) Ag, c) Na, d) Mg, e) Al, f) Si, g) Ca, and h) Ti elements in Ag-ion-exchanged zeolite-TiO_2 catalyst.

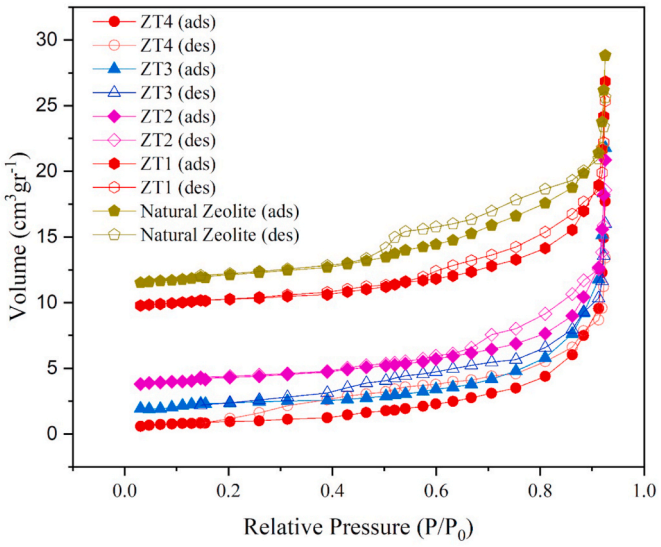

Fig. 8. Nitrogen adsorption–desorption isotherms of natural zeolite and silver ion-exchanged natural zeolite/TiO_2 catalysts.

be concluded that the existence of Ti–O–Si and Ti–O–Al, confirmed by FTIR spectra, could generate positive ion defects, which are electron trappers at the interface of the natural zeolite and deposited TiO_2, because of the combination of Ti^{IV} that is a high positive ion, with the surface oxygen of the natural zeolite framework (Li et al., 2005). This could delay the electron-hole recombination in TiO_2 nanostructures, resulting in an increase in the photoactivity of TiO_2/natural zeolite in comparison to TiO_2 nanoparticles which in turn results in higher antibacterial performance of the catalyst.

Table 2
Data extracted from BET experiments.

Sample	S (m^2g^{-1}) [a]	V (cm^3g^{-1}) [b]	D (nm) [c]
Natural Zeolite	243	0.28	34.15
ZT1	228	0.23	31.36
ZT2	211	0.22	29.55
ZT3	193	0.20	27.87
ZT4	155	0.17	25.54

[a] Calculated with the BET method.
[b] Obtained from BJH desorption.
[c] Obtained from BJH desorption.

3.7. Photodegradation of amoxicillin under UV light

The photocatalytic behavior of bare natural zeolite, ZT1, and ZT3 samples were studied under UV light irradiation. Fig. 10a illustrates the changes in relative concentration (C/C_0) of *AMX* after 5, 15, 30, 50, and 75 min of exposure. As expected, natural zeolite did not show any significant photocatalytic activity. After 75 min of exposure under UV light, approximately 5% of *AMX* was removed, which is consistent with previous reports (Kanakaraju et al., 2015). In addition, it was found that ZT3 sample showed the highest rate of *AMX* degradation, inferring that more concentration of TiO_2 can result in more degradation of *AMX* (Kanakaraju et al., 2015). As *AMX* is known to have high chemical stability, ZT3 sample showed the degradation of *AMX* with a rate constant of 4.89×10^{-3} min^{-1}, which is seven times faster than the photocatalytic activity of bare natural zeolite. Fig. 10b shows the kinetics of *AMX* degradation. The reaction rate constant was calculated using the

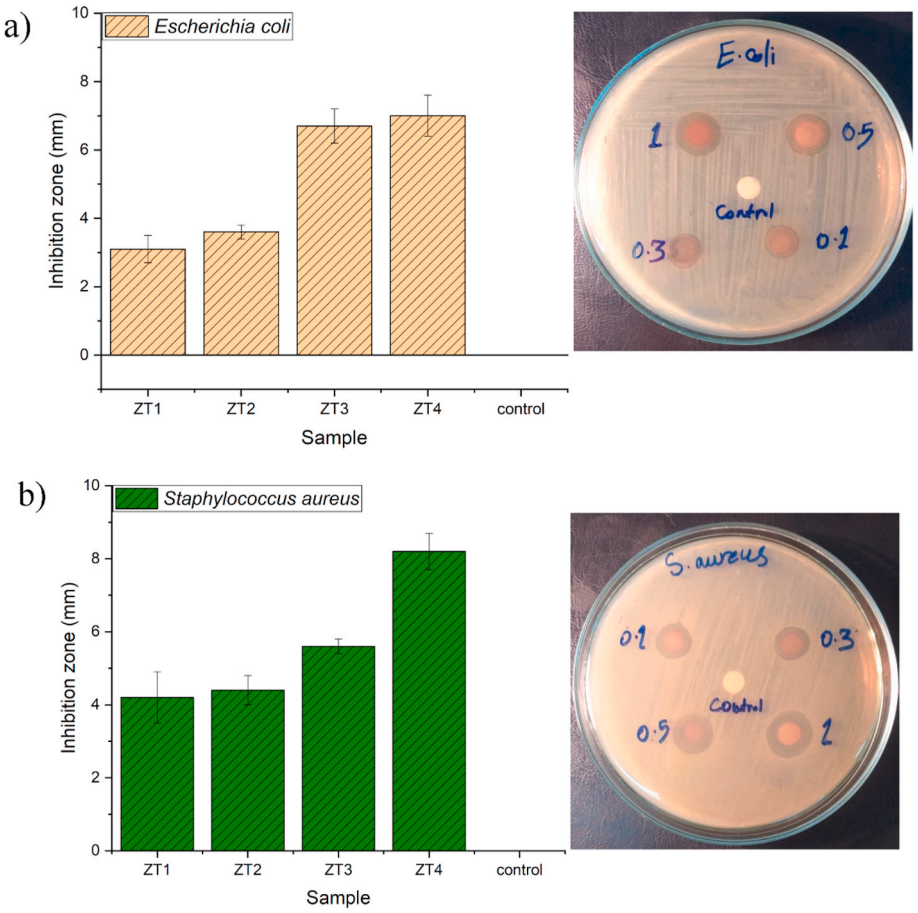

Fig. 9. Antibacterial activity of silver ion-exchanged zeolite-TiO_2 synthesized by hydrolysis of TTIP against a) gram-negative *E. coli* and b) gram-positive *S. aureus*.

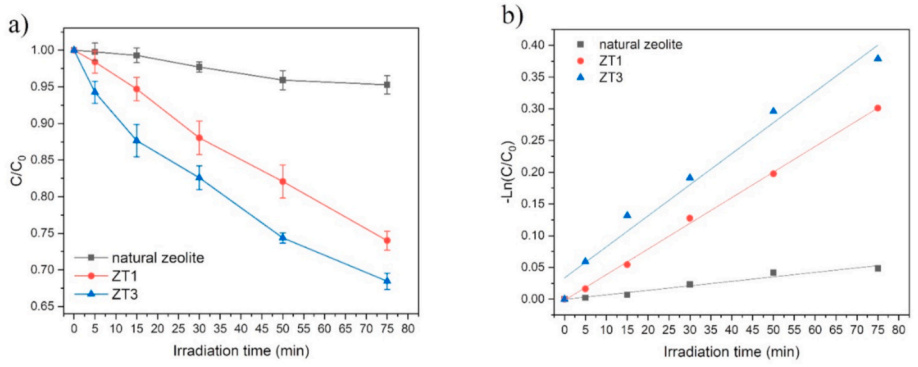

Fig. 10. a) photodegradation of *AMX* and b) First-order kinetic curves of *AMX* degradation, through natural zeolite, ZT1, and ZT3 under UV light.

below equation:

$$\mathrm{Ln}\ (C/C_0) = -k \times t$$

where C is the instant *AMX* concentration, C_0 is the initial *AMX* concentration, *k* is the pseudo-first-order rate constant and, *t* is the reaction time in minutes. The values for the degradation rate constant were concluded to be $7.09 \times 10^{-4}\ min^{-1}$, $4.04 \times 10^{-3}\ min^{-1}$ and $4.89 \times 10^{-3}\ min^{-1}$ for natural zeolite, ZT1 and ZT3, respectively. The better photocatalytic performance of ZT samples, compared with the bare natural zeolite, for the removal of *AMX* from hospital wastewater can be corresponded to two mechanisms. First of all, zeolites are known as electron trappers at the interface of zeolite TiO_2 catalyst, which can reduce charge recombination to some extent. Therefore, the conduction band electrons can be transferred to the surface of zeolite or react with dissolved oxygen so as to produce the superoxide radical $\cdot O_2^-$ while the holes at the TiO_2 are maintained, reacting with the adsorbed *AMX*. This illustrates that zeolite enhances the photocatalytic activity of TiO_2 (PiedraLópez et al., 2021). Secondly, the higher adsorption rate of TiO_2 nanoparticles supported on the zeolite surface is due to the higher adsorption capacity of natural zeolite. This finding confirms the disposal of zeolite particles in integrated photocatalytic adsorbents. The photocatalytic degradation of *AMX* follows 1 to 6 reactions. The degradation of *AMX* has different intermediate products molecules, including CO_2, NH_4^+, and H_2O, and can be due to the hydrolysis of *AMX*. After that, it acts as a nucleophile to the b-lactam ring, followed by ring-opening. Then, it degrades to H_2O and CO_2 (Bergamonti et al., 2019; Klauson

et al., 2010; Song et al., 2016). (see the following equation).

$$AMX + OH^{\bullet} \rightarrow \text{intermediate products} \rightarrow H_2O + CO_2 \quad (6)$$

4. Conclusions

This paper investigates the synthesis and antibacterial and photocatalytic properties of silver-ion-exchanged natural zeolite/TiO_2 catalysts. It aimed to synthesize a low-cost catalyst capable of simultaneously degrading antibiotics and bacteria in wastewater environments, as treating biological and organic contaminants has been one of the biggest challenges in wastewater treatment industry, especially hospital wastewaters. Silver ion-exchanging was performed via the liquid ion-exchange method using 0.1 M $AgNO_3$ solution. Results showed that fine TiO_2 particles have been precipitated on the surface of natural zeolite. Moreover, EDS mapping analysis showed a perfect distribution of Ag in synthesized catalyst samples. The increase in the TiO_2 content of catalyst samples is associated with an increased antibacterial performance of catalysts in both gram-positive *Staphylococcus aureus* ATCC 25923 and gram-negative *Escherichia coli* ATCC 25922. Besides, Ag-containing samples have an improved antibacterial performance in both bacterial conditions.

Author contributions

Niloufar Torkian: Investigation, writing, Conceptualization, Data curation, Formal analysis. Abbas Bahrami: Conceptualization, Supervision, Methodology, Software, Validation, Writing - original draft, Writing - review & editing, Data curation, Formal analysis. Afrouzossadat Hosseini-Abari: Supervision, Methodology, Software, Methodology, Validation, Writing - original draft, Writing - review & editing. Mohammad Mohsen Momeni: Supervision, Methodology, Software, Methodology, Validation, Writing - original draft, Writing - review & editing. Meisam Abdolkarimi-Mahabadi: Methodology, Software, Methodology, Validation, Writing - original draft, Writing - review & editing. Ahmad Bayat: Supervision, Methodology, Software, Methodology, Validation, Writing - original draft, Writing - review & editing. Pejman Hajipour: Investigation, Data curation. Hamed Amini Rourani: Investigation, Writing - original draft, Writing - review & editing. Mohammad Saeid Abbasi: Analysis, Writing - original draft, Writing - review & editing. Sima Torkian: Writing - original draft, Writing - review & editing. Yangping Wen: Supervision, Validation, Writing - review & editing. Maryam Yazdan Mehr: Writing - original draft, Writing - review & editing. Akbar Hojjati-Najafabadi: Supervision, Methodology, Validation, Writing - original draft, Writing - review & editing.

Declaration of competing interest

The authors declare that they have no known competing financial interests or personal relationships that could have appeared to influence the work reported in this paper.

References

Alswat, A.A., Ahmad, M.B., Saleh, T.A., 2017. Preparation and characterization of Zeolite \Zinc oxide-copper oxide nanocomposite: antibacterial activities. Colloids and Interface Science Communications 16, 19–24.

Bai, H., Liu, Z., Sun, D.D., 2011. Hierarchical ZnO/Cu "corn-like" materials with high photodegradation and antibacterial capability under visible light. Phys. Chem. Chem. Phys. 13, 6205–6210.

Bai, H., Liu, Z., Liu, L., Sun, D.D., 2013. Large-scale production of hierarchical TiO2 nanorod spheres for photocatalytic elimination of contaminants and killing bacteria. Chem. Eur J. 19, 3061–3070.

Beier, S., Cramer, C., Köster, S., Mauer, C., Palmowski, L., Schröder, H.F., Pinnekamp, J., 2011. Full scale membrane bioreactor treatment of hospital wastewater as forerunner for hot-spot wastewater treatment solutions in high density urban areas. Water Sci. Technol. 63, 66–71.

Bergamonti, L., Bergonzi, C., Graiff, C., Lottici, P.P., Bettini, R., Elviri, L., 2019. 3D printed chitosan scaffolds: a new TiO2 support for the photocatalytic degradation of amoxicillin in water. Water Res. 163, 114841-114841.

Brundha, C., Karthikeyan, C., Karuppuchamy, S., 2017. Development of nano-structured nano structured TiO 2/CaCO 3 core shell materials for efficient dye-sensitized dye sensitized solar cells. J. Phys. Sci. 1, 76–81.

Cheraghi, A., Davar, F., Homayoonfal, M., Hojjati-Najafabadi, A., 2021. Effect of lemon juice on microstructure, phase changes, and magnetic performance of CoFe2O4 nanoparticles and their use on release of anti-cancer drugs. Ceram. Int. 47, 20210–20219.

Dimitrakopoulou, D., Rethemiotaki, I., Frontistis, Z., Xekoukoulotakis, N.P., Venieri, D., Mantzavinos, D., 2012. Degradation, mineralization and antibiotic inactivation of amoxicillin by UV-A/TiO2 photocatalysis. J. Environ. Manag. 98, 168–174.

Doan, V.-D., Huynh, B.-A., Le Pham, H.A., Vasseghian, Y., 2021. Cu2O/Fe3O4/MIL-101 (Fe) nanocomposite as a highly efficient and recyclable visible-light-driven catalyst for degradation of ciprofloxacin. Environ. Res. 201, 111593.

Foura, G., Chouchou, N., Soualah, A., Kouachi, K., Guidotti, M., Robert, D., 2017. Fe-doped TiO2 supported on HY zeolite for solar photocatalytic treatment of dye pollutants. Catalysts 7, 344-344.

Gawande, M.B., Pandey, R.K., Jayaram, R.V., 2012. Role of mixed metal oxides in catalysis science{\textemdash}versatile applications in organic synthesis. Catalysis Science & Technology 2, 1113-1113.

Ghasemi, S.M., Dormanesh, B., Hosseini Abari, A., Aliasghari, A., Farahnejad, Z., 2018. Comparative characterization of silver nanoparticles synthesized by spore extract of Bacillus subtilis and Geobacillus stearothermophilus. Nanomedicine Journal 5, 46–51.

Hajipour, M.J., Fromm, K.M., Ashkarran, A.A., Aberasturi, D.J.d., Larramendi, I.R.d., Rojo, T., Serpooshan, V., Parak, W.J., Mahmoudi, M., 2012. Erratum: antibacterial properties of nanoparticles. Trends Biotechnol. 30, 499–511. Trends in Biotechnology, 31 (2013) 61-62.

Hajipour, P., Bahrami, A., Eslami, A., Hosseini-Abari, A., Hagh Ranjbar, H.R., 2020. Chemical bath synthesis of CuO-GO-Ag nanocomposites with enhanced antibacterial properties. J. Alloys Compd. 821.

Hajipour, P., Bahrami, A., Mehr, M.Y., van Driel, W.D., Zhang, K., 2021. Facile synthesis of Ag nanowire/TiO2 and Ag nanowire/TiO2/GO nanocomposites for photocatalytic degradation of rhodamine B. Materials 14, 763-763.

Hojjati-najafabadi, A., Davar, F., Enteshari, Z., 2021. Antibacterial and photocatalytic behaviour of green synthesis of Zn 0 . 95 Ag 0 . 05 O nanoparticles using herbal medicine extract. Ceram. Int.

Hojjati Najafabadi, A., Ghasemi, A., Mozaffarinia, R., 2016a. Synthesis and evaluation of microstructural and magnetic properties of Cr3+ substitution barium hexaferrite nanoparticles (BaFe10.5−x Al1.5Cr x O19). J. Cluster Sci. 27, 965–978.

Hojjati Najafabadi, A., Ghasemi, A., Mozaffarinia, R., 2016b. Development of novel magnetic-dielectric ceramics for enhancement of reflection loss in X band. Ceram. Int. 42, 13625–13634.

Hosseini-Abari, A., Emtiazi, G., Lee, S.H., Kim, B.G., Kim, J.H., 2014. Biosynthesis of silver nanoparticles by Bacillus stratosphericus spores and the role of dipicolinic acid in this process. Appl. Biochem. Biotechnol. 174, 270–282.

Huang, Y.z., Ji, Y.r., Kang, Z.w., Li, F., Ge, S.f., Yang, D.P., Ruan, J., Fan, X.q., 2020. Integrating eggshell-derived CaCO3/MgO nanocomposites and chitosan into a biomimetic scaffold for bone regeneration. Chem. Eng. J. 395, 125098-125098.

Jalbani, N.S., Solangi, A.R., Memon, S., Junejo, R., Bhatti, A.A., Yola, M.L., Tawalbeh, M., Karimi-Maleh, H., 2021. Synthesis of new functionalized calix [4] arene modified silica resin for the adsorption of metal ions: equilibrium, thermodynamic and kinetic modeling studies. J. Mol. Liq. 116741.

Kanakaraju, D., Kockler, J., Motti, C.A., Glass, B.D., Oelgemöller, M., 2015. Titanium dioxide/zeolite integrated photocatalytic adsorbents for the degradation of amoxicillin. Appl. Catal. B Environ. 166–167, 45–55.

Karimi-Maleh, H., Shafieizadeh, M., Taher, M.A., Opoku, F., Kiarii, E.M., Govender, P.P., Ranjbari, S., Rezapour, M., Orooji, Y., 2020a. The role of magnetite/graphene oxide nano-composite as a high-efficiency adsorbent for removal of phenazopyridine residues from water samples, an experimental/theoretical investigation. J. Mol. Liq. 298, 112040-112040.

Karimi-Maleh, H., Kumar, B.G., Rajendran, S., Qin, J., Vadivel, S., Durgalakshmi, D., Gracia, F., Soto-Moscoso, M., Orooji, Y., Karimi, F., 2020b. Tuning of metal oxides photocatalytic performance using Ag nanoparticles integration. J. Mol. Liq. 314, 113588.

Karimi-Maleh, H., Karimi, F., Fu, L., Sanati, A.L., Alizadeh, M., Karaman, C., Orooji, Y., 2021a. Cyanazine herbicide monitoring as a hazardous substance by a DNA nanostructure biosensor. J. Hazard Mater. 127058.

Karimi-Maleh, H., Yola, M.L., Atar, N., Orooji, Y., Karimi, F., Kumar, P.S., Rouhi, J., Baghayeri, M., 2021b. A novel detection method for organophosphorus insecticide fenamiphos: molecularly imprinted electrochemical sensor based on core-shell Co3O4@ MOF-74 nanocomposite. J. Colloid Interface Sci. 592, 174–185.

Karimi-Maleh, H., Mousavi, S.J., Mahdavian, M., Khaleghi, M., Bordbar, S., Yola, M.L., Darabi, R., Liu, M., 2021c. Effects of silver nanoparticles added into polyurea coating on sulfate-reducing bacteria activity and electrochemical properties; an environmental nano-biotechnology investigation. Environ. Res. 198, 111251.

Kim, S., Ghafoor, K., Lee, J., Feng, M., Hong, J., Lee, D.U., Park, J., 2013. Bacterial inactivation in water, DNA strand breaking, and membrane damage induced by ultraviolet-assisted titanium dioxide photocatalysis. Water Res. 47, 4403–4411.

Klauson, D., Babkina, J., Stepanova, K., Krichevskaya, M., Preis, S., 2010. Aqueous photocatalytic oxidation of amoxicillin. Catal. Today 151, 39–45.

Lavat, A.E., Grasselli, M.C., 2015. Synthesis and characterization of ceramic materials based on the system MgO-CaO-TiO2 from dolomite. Procedia Materials Science 8, 162–171.

Li, F., Jiang, Y., Yu, L., Yang, Z., Hou, T., Sun, S., 2005. Surface effect of natural zeolite (clinoptilolite) on the photocatalytic activity of TiO 2. Appl. Surf. Sci. 252, 1410–1416.
Li, Q., Jia, R., Shao, J., He, Y., 2019. Photocatalytic degradation of amoxicillin via TiO2 nanoparticle coupling with a novel submerged porous ceramic membrane reactor. J. Clean. Prod. 209, 755–761.
Liao, G., Yao, W., Zuo, J., 2018. Preparation and characterization of zeolite/TiO2 cement-based composites with excellent photocatalytic performance. Materials 11, 2485-2485.
Liu, S., Lim, M., Amal, R., 2014. TiO2-coated natural zeolite: rapid humic acid adsorption and effective photocatalytic regeneration. Chem. Eng. Sci. 105, 46–52.
Mahmoodi, S., Hassan, D.A., Hojjati-Najafabadi, A., Li, W., Liao, L., Moshayedi, A.J., Huang, X., Khajavi, M.N., 2020. Quality enhancement of copper oxide thin film synthesized under elevated gravity acceleration by two-axis spin coating. Ceram. Int. 46, 7421–7429.
Mansoorianfar, M., Rahighi, R., Hojjati-Najafabadi, A., Mei, C., Li, D., 2021. Amorphous/crystalline phase control of nanotubular TiO2 membranes via pressure-engineered anodizing. Mater. Des. 198.
Morones, J.R., Elechiguerra, J.L., Camacho, A., Holt, K., Kouri, J.B., Ramírez, J.T., Yacaman, M.J., 2005. The bactericidal effect of silver nanoparticles. Nanotechnology 16, 2346–2353.
Nadtochenko, V.A., Rincon, A.G., Stanca, S.E., Kiwi, J., 2005. Dynamics of E. coli membrane cell peroxidation during TiO2 photocatalysis studied by ATR-FTIR spectroscopy and AFM microscopy. J. Photochem. Photobiol. Chem. 169, 131–137.
Najafabadi, A.H., Mozaffarinia, R., Rahimi, H., Razavi, R.S., Paimozd, E., 2013. Mechanical property evaluation of corrosion protection. sol – gel nanocomposite coatings 29, 249–254.
Orooji, Y., Tanhaei, B., Ayati, A., Tabrizi, S.H., Alizadeh, M., Bamoharram, F.F., Karimi, F., Salmanpour, S., Rouhi, J., Afshar, S., 2021. Heterogeneous UV-Switchable Au nanoparticles decorated tungstophosphoric acid/TiO2 for efficient photocatalytic degradation process. Chemosphere 281, 130795.
Patterson, A.L., 1939. The scherrer formula for X-ray particle size determination. Phys. Rev. 56, 978–982.
Pelaez, M., Nolan, N.T., Pillai, S.C., Seery, M.K., Falaras, P., Kontos, A.G., Dunlop, P.S.M., Hamilton, J.W.J., Byrne, J.A., O'Shea, K., Entezari, M.H., Dionysiou, D.D., 2012. A review on the visible light active titanium dioxide photocatalysts for environmental applications. Appl. Catal. B Environ. 125, 331–349.
Piedra López, J.G., González Pichardo, O.H., Pinedo Escobar, J.A., de Haro del Río, D.A., Inchaurregui Méndez, H., González Rodríguez, L.M., 2021. Photocatalytic degradation of metoprolol in aqueous medium using a TiO2/natural zeolite composite. Fuel 284, 119030-119030.
Rahman, A., Nurjayadi, M., Wartilah, R., Kusrini, E., Prasetyanto, E.A., Degermenci, V., 2018. Enhanced activity of Tio2/natural zeolite composite for degradation of methyl orange under visible light irradiation. International Journal of Technology 9, 1159–1167.
Ren, C., Yang, B., Wu, M., Xu, J., Fu, Z., lv, Y., Guo, T., Zhao, Y., Zhu, C., 2010. Synthesis of Ag/ZnO nanorods array with enhanced photocatalytic performance. J. Hazard Mater. 182, 123–129.
Sadrnia, A., Orooji, Y., Behmaneshfar, A., Darabi, R., Kamali, D.M., Maleh, H., Opoku, F., Govender, P.P., 2021. Developing a simple box–behnken experimental design on the removal of doxorubicin anticancer drug using Fe3O4/graphene nanoribbons adsorbent. Environ. Res. 111522.
Shahin, K., Bouzari, M., 2018. Bacteriophage application for biocontrolling Shigella flexneri in contaminated foods. J. Food Sci. Technol. 55, 550–559.
Sing, K.S.W., 1985. Reporting physisorption data for gas/solid systems with special reference to the determination of surface area and porosity (Recommendations 1984). Pure Appl. Chem. 57, 603–619.
Song, J., Xu, Z., Liu, W., Chang, C.T., 2016. KBrO3 and graphene as double and enhanced collaborative catalysts for the photocatalytic degradation of amoxicillin by UVA/TiO2 nanotube processes. Mater. Sci. Semicond. Process. 52, 32–37.
Song, H., Yang, G., Song, H.L., Wang, D., Wang, X.Q., 2017. Preparation of Ag/TiO2-zeolite adsorbents, their desulfurization performance, and benzothiophene adsorption isotherms. Russ. J. Phys. Chem. 91, 390–397.
Treacy, M.M.J., Higgins, J.B., 2007. Collection of Simulated XRD Powder Patterns for Zeolites Fifth, Revised Edition. 5th. Collection of Simulated XRD Powder Patterns for Zeolites Fifth (5th) Revised Edition.
Verlicchi, P., Galletti, A., Petrovic, M., BarcelÓ, D., 2010. Hospital effluents as a source of emerging pollutants: an overview of micropollutants and sustainable treatment options. J. Hydrol. 389, 416–428.
Wen, X., Ding, H., Huang, X., Liu, R., 2004. Treatment of hospital wastewater using a submerged membrane bioreactor. Process Biochem. 39, 1427–1431.
Wu, J.J., Tseng, C.H., 2006. Photocatalytic properties of nc-Au/ZnO nanorod composites. Appl. Catal. B Environ. 66, 51–57.
Yue, C., Kuijer, R., Kaper, H.J., Van der Mei, H.C., Busscher, H.J., 2014. Simultaneous interaction of bacteria and tissue cells with photocatalytically activated, anodized titanium surfaces. Biomaterials 35, 2580–2587.
Zhang, G., Song, A., Duan, Y., Zheng, S., 2018. Enhanced photocatalytic activity of TiO2/zeolite composite for abatement of pollutants. Microporous Mesoporous Mater. 255, 61–68.